

Showcasing research from the Kirchner group and the Vöhringer group at the Institute for Physical and Theoretical chemistry, University of Bonn, Germany.

Title: Computing vibrational spectra from *ab initio* molecular dynamics

The paper presents and compares implementations of vibrational spectra computations from *ab initio* molecular dynamics simulations. Mass-weighted power spectra, infrared spectra, and Raman spectra with corresponding depolarization ratios are provided based on time-correlation functions of velocities, dipole moments, and polarizabilities, respectively. Comparison to static calculations and to experimental data is carried out. Furthermore, the applicability to bulk phase systems – which are not directly accessible from static calculations – is demonstrated.

As featured in:



See Kirchner *et al.*,
Phys. Chem. Chem. Phys.,
2013, **15**, 6608–6622.

Computing vibrational spectra from *ab initio* molecular dynamics

Cite this: *Phys. Chem. Chem. Phys.*, 2013, **15**, 6608

Martin Thomas,^{†[a](#)} Martin Brehm,^{†[a](#)} Reinhold Fligg,^b Peter Vöhringer^b and Barbara Kirchner^{†[*a](#)}

We review several methods for the calculation of vibrational spectra from *ab initio* molecular dynamics (AIMD) simulations and we present a new implementation in the trajectory analyzer TRAVIS. In particular, we show mass-weighted power spectra, infrared spectra, and Raman spectra with corresponding depolarization ratios, which are based on time-correlation functions of velocities, dipole moments, and polarizabilities, respectively. Using the four organic molecules methanol, acetone, nitromethane, and pinacol as test systems, we compare the spectra from AIMD simulations of the isolated molecules in gas phase to static calculations relying on the harmonic approximation and to experimental spectra recorded in a nonpolar solvent. The AIMD approach turns out to give superior results when anharmonicity effects are of particular importance. Using the example of methanol, we demonstrate the application to bulk phase systems, which are not directly accessible by static calculations, but for which the AIMD spectra also provide a very good approximation to experimental data. Finally, we investigate the influence of simulation time and temperature in the AIMD on the resulting spectra.

Received 30th November 2012,
Accepted 22nd January 2013

DOI: 10.1039/c3cp44302g

www.rsc.org/pccp

1 Introduction

Vibrational spectroscopy constitutes an important pillar of modern analytical chemistry. The frequencies of molecular vibrations are characteristically determined by the atomic structure, and the presence of certain functional groups can easily be tested. Since the vibrations in a molecule are however not directly visible, different techniques have to be used to investigate them. Two primary examples are infrared (IR) spectroscopy, which is based on the absorption of infrared radiation, and Raman spectroscopy, which relies on the inelastic scattering of usually visible light. Many more methods in the spirit of these ideas have been developed, and by this means, vibrational spectra have been shown to serve as molecular fingerprints. They are therefore an important tool *e.g.* in chemical structure determination and bioanalytical applications.^{1–8}

The theoretical prediction of vibrational spectra is a well established field of computational chemistry today.^{9–30}

The first step in such studies is always the calculation of the vibrational normal modes of the molecule. In the most basic approach, this is carried out within the harmonic approximation. This means that the potential energy surface is assumed to behave like a harmonic potential in the local neighborhood of a minimum obtained by geometry optimization and the vibrational frequencies are directly derived from the second derivatives of the potential energy. Although this method works very well in many cases, it neglects anharmonicities and empirical scaling factors are often introduced to overcome this issue.^{31–33} However, more sophisticated techniques for anharmonic effects have also been described.^{11–13,19,21,22,27,28} In any case, the intensities for IR and Raman spectra are obtained from the derivatives of the dipole moment and the polarizability, respectively, along the normal mode vectors in such static calculations.³⁰ The derivation can be performed numerically^{9,30} by using finite differences, but analytical techniques are also available.^{34,35}

A major issue in the estimation of vibrational spectra by static calculations is the solvent influence. The interaction with solvent molecules is known to be important in many cases, particularly when hydrogen bonds between the solvent and the analyte can be formed.^{36–38} Since static calculations need to be started from an optimized minimum of the potential energy surface, they are usually applied to isolated molecules in gas phase,

^a Wilhelm-Ostwald-Institut für Physikalische und Theoretische Chemie, Universität Leipzig, Linneestr. 2, D-04103 Leipzig, Germany.

E-mail: bkirchner@uni-leipzig.de; Fax: +49 341 9736399; Tel: +49 341 9736401

^b Institut für Physikalische und Theoretische Chemie,

Rheinische Friedrich-Wilhelms-Universität, Wegelerstr. 12, D-53115 Bonn, Germany

† Present address: Mulliken Center for Theoretical Chemistry, Rheinische Friedrich-Wilhelms-Universität, Beringstr. 4, D-53115 Bonn, Germany.

where such minima are easier to find, but the solvent influence is totally missed then. A partial improvement is possible by continuum solvation models. Although these can model the general electrostatic environment, they are still unable to describe specific interactions like *e.g.* hydrogen bonds between the solvent and the analyte. In such cases, it is necessary to explicitly include the solvent molecules in the electronic structure calculation. Microsolvation techniques can potentially be used in connection with static calculations,^{39,40} but the explicit calculation of all vibrational normal modes becomes computationally very demanding in this way. A general simulation of the bulk phase requires therefore to switch to *ab initio* molecular dynamics (AIMD),^{41–50} where different configurations of the phase space can easily be sampled, while at the same time, the electronic structure is treated.

The prediction of vibrational spectra by AIMD requires the application of new methods because derivatives of the dipole moment and the polarizability are not directly available anymore. The first step towards the calculation of vibrational spectra is therefore the power spectrum, which is obtained by a Fourier transform of the autocorrelation of the particle velocities.⁵¹ The power spectrum features peaks at all vibrational frequencies of the system and it can also be understood as a vibrational density of states. It is also possible to extract vibrational normal modes from power spectra.^{52,53} In a similar manner, IR spectra can be calculated from the autocorrelation of the molecular dipole moment and Raman spectra are determined from the autocorrelation of the molecular polarizability. Besides providing the possibility to study systems in the bulk phase, the spectra from AIMD intrinsically account for certain anharmonicity effects, since no assumptions about the shape of the potential energy surface—such as the harmonic approximation in static calculations—are made. However, other anharmonicity influences like mode coupling leading to combination bands and Fermi resonances are still not included.^{54,55} For convenience, we refer to the potential energy surface shape effect simply as anharmonicity here, although the latter issues are not specifically addressed in our approach.

Several examples for the calculation of vibrational spectra from AIMD have already been reported in the literature.⁴² Among others, these include the IR spectra of different water modifications investigated by Silvestrelli *et al.*^{56,57} and Iftimie and Tuckerman,⁵⁸ the IR spectra of hydrogen chloride hydrates explored by Buch and coworkers,^{59–61} as well as the IR spectra of several biologically relevant molecules studied by Gaigeot and coworkers.^{62–67} In all these cases, the dipole moment under periodic boundary conditions was calculated either by the Berry phase approach to polarization^{68,69} or by the maximally localized Wannier function scheme.^{70–73} Applications to peptide systems using dipole moments from atomic population analysis have been reported by Cho and coworkers.^{74,75} Also the prediction of Raman spectra has been described *e.g.* by Aida and Dupuis for a single D₂O molecule⁷⁶ and by Miani and coworkers for clavulanic acid⁷⁷ and β-lactamase inhibitors⁷⁸ in aqueous solution modeled by a QM/MM scheme. In these studies, the polarizability was obtained using standard quantum

chemistry program packages, for which certain parts of the aqueous solution systems had to be cut out and an electronic structure method different from the one for the dynamics was employed.^{79,80} An analytic technique to calculate polarizabilities within perturbation theory for periodic systems has been described by Putrino *et al.*,⁸¹ and it has been applied to different systems.^{82–84} A study on the choice of the simulation timestep and the energy distribution between normal modes has been performed by Horníček *et al.*⁵⁴

In this work, we present the implementation in our trajectory analyzer TRAVIS⁸⁵ to calculate power spectra, IR spectra and Raman spectra from AIMD simulations. Our approach for IR and Raman intensities is thoroughly based on the maximally localized Wannier function scheme, which allows for direct calculation of individual molecular dipole moments also in bulk phase systems under periodic boundary conditions. Furthermore, we demonstrate our method for the calculation of individual molecular polarizabilities in such systems, which utilizes the change in the molecular dipole moments due to the application of an external electric field. This permits the estimation of all the vibrational spectra on the same level of theory. As simple test systems, we have chosen the small organic molecules methanol, acetone, nitromethane and pinacol to examine several different functional groups. For these molecules, we compare our results to static calculations and to experimental data. To demonstrate the applicability of our methodology to liquid systems, we also show a methanol bulk phase. Finally, we investigate the influence of the temperature within the AIMD simulation and the total simulation length on the resulting spectra.

2 Theoretical background

2.1 Autocorrelation functions

All vibrational spectra calculated from AIMD are based on the Fourier transform of certain autocorrelation functions: power spectra use the particle velocities, IR spectra rely on molecular dipole moments and Raman spectra are obtained from molecular polarizabilities. It is therefore important to efficiently calculate autocorrelation functions and their Fourier transform, since direct application of the definition leads to an algorithm scaling with $\mathcal{O}(n^2)$. However, the Wiener–Khintchine theorem^{86,87} shows that the autocorrelation of a function $f(t)$ is given by

$$\langle f(\tau)f(t+\tau) \rangle_\tau = \frac{1}{2\pi} \int \left| \int f(t) e^{-i\omega t} dt \right|^2 e^{i\omega \tau} d\omega, \quad (1)$$

so that the Fourier transform of $f(t)$ is taken, its square is calculated in the frequency domain, and the inverse transformation is applied. By using the fast Fourier transform algorithm, this calculation scheme scales with $\mathcal{O}(n \log n)$.

2.2 Power spectra

The simplest way to obtain a vibrational spectrum from an AIMD trajectory is the power spectrum, since it only relies on

the nuclear velocities, which are always known during a molecular dynamics simulation, given the right algorithms are used. For each atom, the vector autocorrelation of the velocity is calculated and the sum of all the correlation functions of a molecule is Fourier transformed to get the power spectrum of that molecule.⁸⁸ This power spectrum features peaks for each normal mode vector and allows investigation of vibrational frequencies independently of IR and Raman selection rules.

An interesting quantity in this context is the intensity of the peaks in a power spectrum. A simple example to approach this is a system containing only harmonic oscillators. If a classical molecular dynamics simulation of this system is well equilibrated, the equipartition theorem is fulfilled, so that each of the oscillators contains the same amount of energy.⁸⁹ Under these conditions, it follows from the laws of classical physics that the amplitude is inversely proportional to the eigenfrequency ω and inversely proportional to the square root of the reduced mass m . The autocorrelation of the oscillator elongations is a superposition of all the oscillations with the different eigenfrequencies so that the Fourier transform creates a spectrum with a peak at each eigenfrequency. The intensities of these peaks are determined by the corresponding oscillator amplitudes. Since products of the positions enter the autocorrelation, a spectrum with the same intensity for each oscillator is obtained by rescaling the Fourier transform according to

$$P(\omega) = m\omega^2 \int \langle \mathbf{r}(\tau)\mathbf{r}(t+\tau) \rangle_{\tau} e^{-i\omega t} dt, \quad (2)$$

where $\langle \mathbf{r}(\tau)\mathbf{r}(t+\tau) \rangle_{\tau}$ denotes the autocorrelation of the positions \mathbf{r} . Following from the properties of the Fourier transform, it is formally equivalent to use

$$P(\omega) = m \int \langle \dot{\mathbf{r}}(\tau)\dot{\mathbf{r}}(t+\tau) \rangle_{\tau} e^{-i\omega t} dt, \quad (3)$$

but this expression is advantageous due to numerical reasons. The $\dot{\mathbf{r}}$ describes the time derivative of the position so that eqn (3) is the Fourier transform of the previously mentioned velocity autocorrelation, which is however rescaled by the reduced mass of the oscillator. Consequently, this means that the intensity is inversely proportional to the reduced mass in a power spectrum calculated from the velocity autocorrelation in a molecular dynamics simulation.

Following the derivation in the last paragraph, it is convenient to create mass-weighted power spectra from an AIMD trajectory, where for each atom the velocity autocorrelation is multiplied by the atomic mass. If all vibrations were purely harmonic, each peak in the spectrum would have the same intensity (*i.e.* the integral of the peak), as long as the system follows the equipartition theorem. This would provide a nice possibility to check whether the simulation was well equilibrated. In reality however, all vibrations suffer from anharmonic effects^{11–13,19,21,22,27,28} so that this condition cannot strictly be fulfilled. The anharmonicity causes a broadening of the bands and it influences the intensities. Furthermore, the normal modes are often very close in energy in a real-world system so that the corresponding peaks will be overlapping in the power spectrum.

Nevertheless, the intensity in the mass-weighted power spectrum is still a very helpful tool for qualitative conclusions.

2.3 IR and Raman intensities

The calculation of IR and Raman intensities is usually based on the appropriate quantum mechanical expressions for absorption and scattering of light, which are derived using time-dependent perturbation theory. Starting from these, it can be shown in the time-correlation function formalism⁸⁹ that the IR absorption coefficient and the Raman scattering cross section are proportional to the autocorrelation of the dipole moment and the polarizability, respectively. The resulting equations however rely on the ensemble averages of the corresponding quantum mechanical operators, so they are not directly applicable to standard AIMD, where the nuclei move according to the classical equations of motion. Several different approaches to connect the classical correlation function obtainable from AIMD to the quantum mechanical correlation function have been discussed in the literature (see ref. 90 and 91 for details and ref. 56, 58 and 62 for discussions thereof). In the following paragraphs, another way to approach this problem is described, which finally leads however to the same proportionalities as previous methods.

In static calculations, the intensities are obtained from derivatives of the dipole moment and the polarizability along the vibrational normal modes. By this means, the integral IR absorption coefficient $\mathcal{A}_{\tilde{\nu}}$ of normal mode p is given by³⁰

$$\mathcal{A}_{\tilde{\nu}} = \frac{1}{4\pi\epsilon_0} \frac{N_A \pi}{3c^2} \left(\frac{\partial \mu}{\partial Q_p} \right)^2, \quad (4)$$

where Q_p denotes the mass-weighted normal coordinate corresponding to normal mode p , N_A is Avogadro's constant, c is the speed of light, and ϵ_0 is the vacuum permittivity. The derivative of the dipole moment has to be evaluated at the equilibrium geometry. The situation is more complex for the Raman intensity, since also the scattering geometry needs to be specified in this case. We consider only the typical setup of an incident beam propagating in the y direction with polarization along the x axis and detection of the scattered light in the z direction here. Nevertheless, extensions to other experimental geometries should be straightforward. Following the derivations of Long,⁹² the Raman scattering intensity I_{\parallel} of space fixed molecules for detection of x polarized light in this case is given by

$$I_{\parallel} = \frac{\pi^2}{\epsilon_0^2} (\tilde{\nu}_{in} - \tilde{\nu}_p)^4 \frac{hN\mathcal{I}}{8\pi^2 c \tilde{\nu}_p} \left(\frac{\partial \alpha_{xx}}{\partial Q_p} \right)^2 \frac{1}{1 - \exp\left(-\frac{h\tilde{\nu}_p}{k_B T}\right)}, \quad (5)$$

where $\tilde{\nu}_{in}$ is the wavenumber of the incident light, $\tilde{\nu}_p$ is the wavenumber of normal mode p , N is the number of molecules, \mathcal{I} is the irradiance of the incident light, h is Planck's constant, k_B is Boltzmann's constant, and T is the temperature. The derivative again has to be evaluated at the equilibrium geometry. The same expression holds for the intensity I_{\perp} of the detection of y polarized light if the polarizability tensor element

α_{xx} is replaced by α_{xy} . Another important quantity in this context is the depolarization ratio $\rho = I_{\perp}/I_{\parallel}$, which is defined as the ratio of these two contributions. It can be lower than 0.75 for totally symmetric normal modes, but it is 0.75 in all other cases. If the random orientation of the molecules with respect to the laboratory coordinate system is considered, the appropriate averages lead to

$$I_{\parallel} \propto \frac{(\tilde{\nu}_{in} - \tilde{\nu}_p)^4}{\tilde{\nu}_p} \frac{45a_p^2 + 4\gamma_p^2}{45} \frac{1}{1 - \exp\left(-\frac{hc\tilde{\nu}_p}{k_B T}\right)} \quad (6)$$

for detection of x polarized light and

$$I_{\perp} \propto \frac{(\tilde{\nu}_{in} - \tilde{\nu}_p)^4}{\tilde{\nu}_p} \frac{3\gamma_p^2}{45} \frac{1}{1 - \exp\left(-\frac{hc\tilde{\nu}_p}{k_B T}\right)} \quad (7)$$

for detection of y polarized light, where the isotropic polarizability

$$a_p = \frac{1}{3} \left(\frac{\partial \alpha_{xx}}{\partial Q_p} + \frac{\partial \alpha_{yy}}{\partial Q_p} + \frac{\partial \alpha_{zz}}{\partial Q_p} \right) \quad (8)$$

and the anisotropy

$$\begin{aligned} \gamma_p^2 &= \frac{1}{2} \left(\frac{\partial \alpha_{xx}}{\partial Q_p} - \frac{\partial \alpha_{yy}}{\partial Q_p} \right)^2 + \frac{1}{2} \left(\frac{\partial \alpha_{yy}}{\partial Q_p} - \frac{\partial \alpha_{zz}}{\partial Q_p} \right)^2 \\ &\quad + \frac{1}{2} \left(\frac{\partial \alpha_{zz}}{\partial Q_p} - \frac{\partial \alpha_{xx}}{\partial Q_p} \right)^2 + 3 \left(\frac{\partial \alpha_{xy}}{\partial Q_p} \right)^2 \\ &\quad + 3 \left(\frac{\partial \alpha_{yz}}{\partial Q_p} \right)^2 + 3 \left(\frac{\partial \alpha_{zx}}{\partial Q_p} \right)^2 \end{aligned} \quad (9)$$

are defined.

In an AIMD simulation, the derivatives of the dipole moment and the polarizability along the normal modes are not directly available. The time-correlation functions provide however another way to access the same information. In the AIMD, all vibrational normal modes are excited at once, so that the time-dependent oscillations of the dipole moment and the polarizability contain contributions from all normal modes at the same time. Since each of these contributions oscillates at the frequency of the corresponding normal mode, the spectrum of all active normal modes is obtained at once by a Fourier transform of the correlation function. The intensity of this spectrum corresponds to the amplitude of the oscillation in the correlation function so that large changes in the dipole moment or the polarizability lead to a large peak in the spectrum and *vice versa*. It is therefore possible to replace the derivatives along the normal modes by the corresponding correlation functions in the expressions of static calculations. In doing so, it has to be kept in mind that according to the equipartition theorem not all vibrations will have the same amplitude in the AIMD simulation so that the intensities in the spectrum need to be scaled properly. As it has already been discussed for the power spectra, a simple approach to this issue follows from the assumption that all vibrations are harmonic so that we again introduce the harmonic approximation for IR and Raman intensities here. Since the amplitude of a distinct

normal mode in mass-weighted coordinates is inversely proportional to the eigenfrequency ω , the oscillations of the dipole moment and the polarizability are scaled by $1/\omega$. Because products of these quantities enter the correlation functions, the spectrum after the Fourier transform needs to be multiplied by ω^2 . As described for the power spectra, it is convenient to use the time derivatives instead, so that the IR intensity is given by

$$A(\omega) \propto \int \langle \dot{\mu}(\tau) \dot{\mu}(t + \tau) \rangle_t e^{-i\omega t} dt. \quad (10)$$

In a similar manner, we replace the derivative in eqn (5) by the autocorrelation of the polarizability to get the parallel polarized Raman intensity for fixed molecular orientation. In contrast to the IR intensity, there are additional terms depending on the vibrational frequency so that the expression becomes

$$I_{\parallel}(\omega) \propto \frac{(\omega_{in} - \omega)^4}{\omega} \frac{1}{1 - \exp\left(-\frac{\hbar\omega}{k_B T}\right)} \int \langle \dot{\alpha}_{xx}(\tau) \dot{\alpha}_{xx}(t + \tau) \rangle_t e^{-i\omega t} dt. \quad (11)$$

The formula for $I_{\perp}(\omega)$ is completely analogous with α_{xx} replaced by α_{xy} . If the average over all molecular orientations is considered, each squared term in the isotropic contribution a_p^2 and the anisotropic contribution γ_p^2 has to be replaced by the corresponding autocorrelation function, and the Raman intensities finally follow from eqn (6) and (7).

2.4 Dipole moments and polarizabilities

As shown in the last section, the intensities for IR and Raman spectra rely on molecular dipole moments and polarizabilities, so an efficient scheme to obtain these from AIMD simulations is necessary. Two different methods to calculate the dipole moment under periodic boundary conditions have been discussed in the literature: the Berry phase approach to polarization^{68,69} and the maximally localized Wannier function scheme.^{70–73} The former provides the total dipole moment of the simulation box and this is perfectly suited as long as only a single molecule is simulated. In the bulk phase however, it does not allow us to analyze the individual molecular contributions to the dipole moment. In this case it is more convenient to use the maximally localized Wannier function scheme. By a unitary transformation of the Kohn-Sham orbitals, this technique produces a set of localized Wannier orbitals whose position expectation values r_i (the Wannier function centers) can be interpreted as the locations of electron pairs. In the bulk phase, the Wannier function centers can be assigned to individual molecules by a minimum distance criterion and the molecular dipole moment μ is calculated by summing electronic and nuclear contributions as in

$$\mu = -2e \sum_i r_i + e \sum_j Z_j \mathbf{R}_j, \quad (12)$$

where \mathbf{R}_j denotes the nuclear positions and Z_j their charges. Generally, this definition is not unique any more as soon as the molecule is charged. In this case, the choice of the reference

point for the \mathbf{r}_i and \mathbf{R}_j affects the dipole moment,⁴⁵ but this does not matter here, because only time-derivatives of the dipole moment are used and the core charges are constant in time. The formula individually provides the dipole moment of all the molecules in a bulk phase under the influence of the surrounding molecules, given that the localization procedure converges. Apart from the explicit consideration of bulk phase effects on the spectrum, this also improves the sampling compared to the simulation of an isolated molecule. Furthermore, this gives the possibility to study the pure spectrum of a solute molecule interacting with the solvent.⁹³

The molecular polarizability needed for Raman intensities requires more computational effort than the dipole moment. A possible calculation scheme starts with the dipole moment induced by an external electric field \mathbf{E} . As long as nonlinear effects occurring at high field strengths are neglected, this induced dipole is given by

$$\mu_{\text{ind}} = \alpha E, \quad (13)$$

where α is the polarizability tensor. Following this equation, it is possible to calculate the polarizability from the change in the dipole moment caused by an external electric field *via* finite differences. If the dipole moments are obtained again using the maximally localized Wannier function scheme, this provides the polarizability for each individual molecule. For every desired timestep of the AIMD trajectory, the procedure requires additional single-point calculations where an electric field is applied. To get all tensor components of the polarizability, the electric field needs to be applied along each of the three independent directions of space, so this results in three single-point calculations for one timestep. As long as isotropic systems are simulated, every possible molecular orientation with respect to the box coordinate system should appear in the AIMD trajectory if the simulation runs sufficiently long, so it is not mandatory to use the orientational averaging procedure of eqn (6) and (7) in this case. This would reduce the number of single-point calculations per timestep to one because only α_{xx} and α_{xy} are needed (see eqn (11)), but it would also affect the sampling and therefore the quality of the spectra.

3 Methodology

3.1 Computational details

The AIMD simulations were performed using the Quickstep module⁹⁴ of the CP2K program package,⁹⁵ where the orbital transformation⁹⁶ method was applied for faster convergence. Density functional theory was used as an electronic structure method utilizing the BLYP exchange-correlation functional^{97,98} with Grimme's dispersion correction D3.⁹⁹ The molecularly optimized double-zeta basis set (MOLOPT-DZVP-SR-GTH)¹⁰⁰ was applied to all atoms together with the corresponding Goedecker-Teter-Hutter (GTH) pseudopotentials.^{101–103} A timestep of 0.5 fs was chosen and the temperature was set to 400 K using a Nosé–Hoover chain thermostat.^{104–106} Starting from optimized geometries of the individual molecules, the systems were equilibrated using the massive thermostat option

(individual thermostat for each degree of freedom) for 3 ps. The production simulations were subsequently run for 30 ps. An electric field strength of $2.57 \times 10^8 \text{ V m}^{-1}$ was used in the calculation of the polarizabilities at every fifth timestep of the trajectory, and the Raman intensities were evaluated for an incident laser wavelength of 514 nm.

The static calculations were carried out using TURBOMOLE 6.0.¹⁰⁷ Density functional theory was applied within the RI approximation^{108–112} utilizing again the BLYP exchange-correlation functional^{97,98} with Grimme's dispersion correction D3⁹⁹ to estimate harmonic frequencies, IR intensities, and Raman intensities.^{35,113–115} A polarized triple-zeta basis set (def2-TZVP)¹¹⁶ was used for all atoms. In all cases, isolated molecules in gas phase were used and the frequency and intensity calculations were preceded by a full geometry optimization.

The methodology to calculate power, IR, and Raman spectra is available in TRAVIS⁸⁵ and, to some extent, already has been used for certain applications before.^{46–48,88} All AIMD-based spectra shown in this article have been computed with TRAVIS. The implementation is based on eqn (1), (3), (10), and (11). The molecular dipole moments are determined from the maximally localized Wannier function centers according to eqn (12) using a minimum distance criterion to assign the Wannier function centers to individual molecules. The resulting dipole vectors are used to calculate molecular IR spectra as in eqn (10) and molecular polarizabilities needed for Raman spectra based on eqn (13). Apart from this rationale, some more sophisticated methods—like application of a window function, zero padding, and fast autocorrelation using the Wiener–Khintchine theorem (see Section 2.1 and ref. 85)—are utilized. Altogether, this yields a fast and reliable framework for the calculation of spectra from AIMD simulations. All diagrams presented in this article have been created using the Xmgrace¹¹⁷ plotting software.

3.2 Experimental setup

Fourier transform IR spectra were recorded using a commercial spectrometer (Nicolet 5700, Thermo Fisher) with a spectral resolution of about 2 cm^{-1} . Dilute liquid solutions were held in sample cells that had an optical path length of 2 mm and that were sealed with CaF₂ windows for transmission measurements. Neat liquids were measured in attenuated total internal reflection mode using a diamond prism allowing for an effective optical path length of about 2 microns. All chemicals were purchased from Sigma Aldrich. Pinacol (98%) was dried under vacuum for several days, methanol (anhydrous, 99.8%) was dried by storage for several days over a molecular sieve (Roth, 0.3 nm pore size), and smaller quantities of carbon tetrachloride (25 mL, CHROMASOLV, >99.9%) were dried by irradiation for 15 minutes in a microwave field (power 100 W, CEM, Discover SP).

4 Results and discussion

In the following sections, we present the results for our four test molecules methanol, acetone, nitromethane and pinacol. For all these molecules, we show mass-weighted power spectra,

IR spectra, and Raman spectra obtained from AIMD simulations, and we compare them to static calculations within the harmonic approximation. In doing so, we shortly denote the spectra obtained from the static calculations as static spectra and we refer to the frequencies yielded from the static calculations as static frequencies. In the power spectra, we can only relate the peak positions to the static frequencies, but we can also analyze the intensities of the individual bands in the IR spectra, and we can additionally discuss the depolarization ratios in the Raman spectra. Finally, we compare the simulation results to experimental data.

4.1 Methanol

The spectra obtained for a single methanol molecule are shown in Fig. 1. The power spectrum should feature peaks exactly at the positions of the vibrational normal modes, which is nicely fulfilled here. The band corresponding to the C–H stretching vibrations around 3000 cm^{-1} is slightly shifted to higher frequencies and the H–C–O–H torsional mode below 300 cm^{-1} appears at slightly lower frequencies as compared to the harmonic normal mode analysis. However, the positions of all remaining normal modes agree very well. Nevertheless, slight deviations in the frequencies have to be expected due to the differences in the underlying electronic structure model since the basis sets are different and periodic boundary conditions are applied in the AIMD simulations. The broadening of the O–H stretching band at 3700 cm^{-1} furthermore indicates that anharmonicity is of particular importance for this vibration.

Comparing the IR spectrum obtained from static calculations to the one from AIMD, the overall shape agrees very well. For each normal mode with significant IR intensity in the static calculation, there is a corresponding peak in the AIMD spectrum. In the region between 1000 cm^{-1} and 1500 cm^{-1} also the intensity ratios are in very good agreement. Furthermore, it has to be kept in mind that the width of the Lorentzian functions in the static spectrum can arbitrarily be chosen so that it is not possible to correctly predict the width of the peaks there. Nevertheless, the integrated intensity needs to be the same so the low frequency band at 300 cm^{-1} , corresponding to the torsion of the C–O bond, also fits well. In the region of the C–H stretching vibrations around 3000 cm^{-1} , the AIMD spectrum shows only a single peak whereas all three normal modes are IR active there. However, the power spectrum indicates that these three normal modes are difficult to separate in the AIMD because they are obviously very close in frequency, so that their intensity is merged in the IR spectrum from AIMD. The major difference remains the intensity of the O–H stretching vibration observed at 3700 cm^{-1} , which is much lower in the static spectrum. Potentially, this is caused by the basis set difference, but more likely it is due to the total neglect of anharmonicities in the static calculation. The importance of anharmonicity for this vibration is also indicated by its broadening in the power spectrum.

Also the overall shapes of the Raman spectra agree very well. For each Raman active normal mode, there is a corresponding band in the AIMD spectrum. The intensities match in most cases,

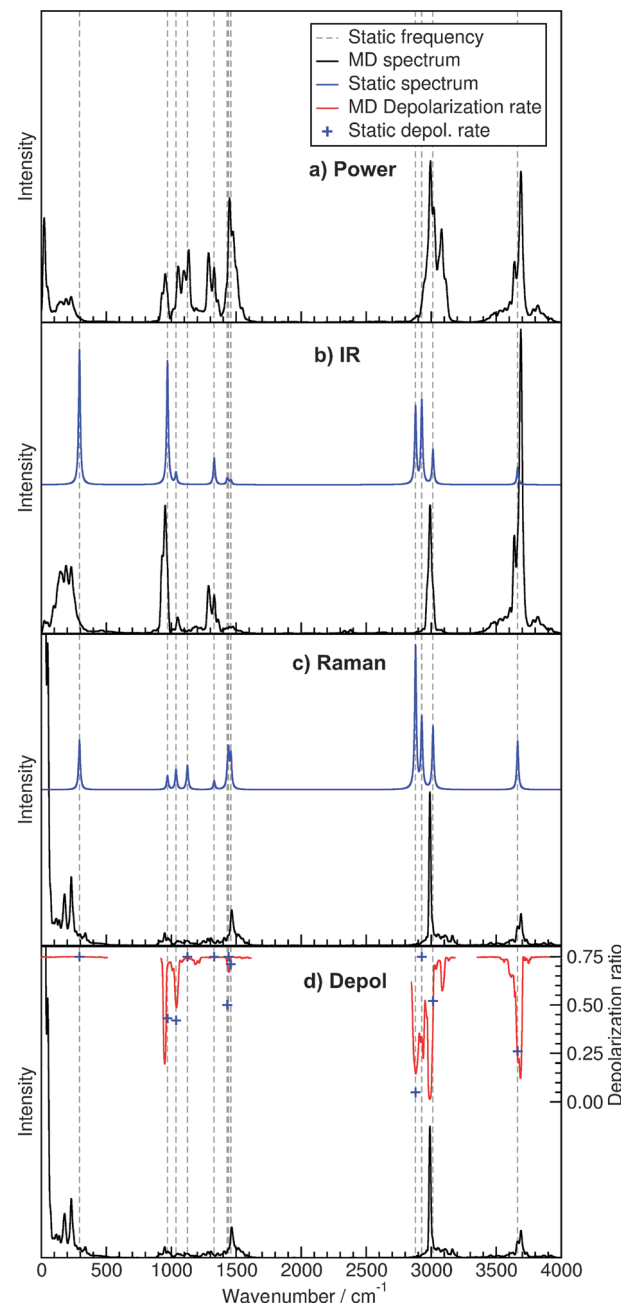


Fig. 1 Spectra for a single methanol molecule (normal modes from static calculation indicated by dashed vertical lines, static spectra broadened by Lorentzian functions with FWHM of 15 cm^{-1}): (a) power spectrum from AIMD simulation; (b) IR spectra from AIMD simulation and static calculation; (c) Raman spectra from AIMD simulation and static calculation; (d) Raman depolarization ratios from AIMD simulation and static calculation (indicated by crosses) with Raman spectrum from AIMD simulation.

but there seem to be some differences for the C–H deformation modes at 1040 cm^{-1} and 1120 cm^{-1} . The broad distribution of the Raman intensity in this frequency region indicates however that this is probably an anharmonicity effect. A further deviation is again found for the C–H stretching vibrations around 3000 cm^{-1} , where the AIMD spectrum features only one pronounced peak instead of three, but the same reasoning as for

the IR spectra holds also for the Raman spectra. Another important finding in the AIMD spectrum is the very large peak at zero frequency, which corresponds to the rotation of the molecule. As long as the molecule is not of spherical symmetry, the polarizability changes with respect to the laboratory coordinate system due to the rotation, which is always active in an AIMD simulation. However, it is not possible to derive rotational Raman spectra from that, because the rotation is not quantized in the standard AIMD.

An important quantity closely connected to the Raman intensity is the depolarization ratio. Because it is defined as the ratio of two spectra, it is obtained over the whole frequency range from the AIMD simulation. However, it is meaningful only as long as significant Raman intensity is present, so we only show the depolarization ratio for these regions and compare it to the values given by the static calculation. The differences between the two methods are more pronounced than those for the spectra itself, but the predictions are qualitatively still in good agreement. Considering the previously discussed frequency shift of the C-H stretching vibrations, these and also the O-H stretching mode fit very well. Furthermore, the static calculation predicts three polarized bands between 900 cm^{-1} and 1500 cm^{-1} , and these are also found in the AIMD. Finally, both methods agree on the depolarization ratio of the low frequency mode at 300 cm^{-1} .

The experimental IR spectrum of methanol in carbon tetrachloride is shown in Fig. 2. Due to the low solubility of

methanol in carbon tetrachloride and to avoid the formation of methanol clusters, a thick layer with low methanol concentration was measured so that the region below 2000 cm^{-1} is totally covered by the solvent bands. Therefore, it is possible to analyze only the stretching modes of the C-H and O-H bonds. A comparison to the AIMD spectrum and the static calculation shows that the frequencies are slightly overestimated in both cases, which is very likely a deficiency of the exchange-correlation functional in the underlying electronic structure method. However, it can also be connected to the neglect of improper hydrogen bonding.¹¹⁸ Although the AIMD simulation is not able to recover the shape of the C-H stretching band, it performs definitely better than the static calculation when the peak of the O-H stretching vibration and its relative amplitude with respect to the C-H stretching mode are considered. This further confirms that the inclusion of anharmonicity is of particular importance for this normal mode. The AIMD spectrum below 2000 cm^{-1} compares well to literature data.¹¹⁹

To demonstrate the applicability of the methodology to bulk phases, we also simulated a system of 16 methanol molecules. The corresponding spectra are presented in Fig. 3. The power spectrum looks similar to the one of the single methanol molecule. Most of the peaks are at the same positions although the single molecule bands between 1300 cm^{-1} and 1500 cm^{-1} are fused now. A very important difference concerns however the O-H stretching mode, which was connected to a sharp peak at 3700 cm^{-1} for the single molecule. In the bulk phase, this vibration causes a very broad band between 3000 cm^{-1} and 3500 cm^{-1} . This nicely shows the influence of hydrogen bonding in liquid methanol, which is automatically included in the bulk phase AIMD simulation, but completely neglected in the single molecule calculation. Another broad peak connected to the intermolecular interactions shows up around 650 cm^{-1} , which is totally missing in the single molecule spectrum.

The prominent influence of hydrogen bonding is also seen in the IR spectra. Similar to the power spectra, the sharp O-H stretching peak at 3700 cm^{-1} is replaced by a very broad band between 2800 cm^{-1} and 3600 cm^{-1} . Furthermore, another broad band connected to the intermolecular interactions emerges at around 650 cm^{-1} . This is a very much satisfying result since these two effects are essential features of the experimental IR spectrum of liquid methanol (see Fig. 2 and ref. 119–121). In addition, the narrow shapes of the remaining peaks observed in the experiment are also reproduced well, so that finally the AIMD trajectory of only 16 methanol molecules provides a very good approximation to the experimental results for liquid methanol.

The influence on the O-H stretching vibration is also visible in the Raman spectrum, although it is less pronounced there due to the lower Raman activity of this normal mode. The remaining parts of the Raman spectrum are similar to the single molecule case, only the band at 230 cm^{-1} vanishes. Also the depolarization ratios predicted for the bulk phase are almost the same as in the single molecule calculation except for the peak broadening effects. In any case, the AIMD trajectory containing 16 methanol molecules finally provides a very

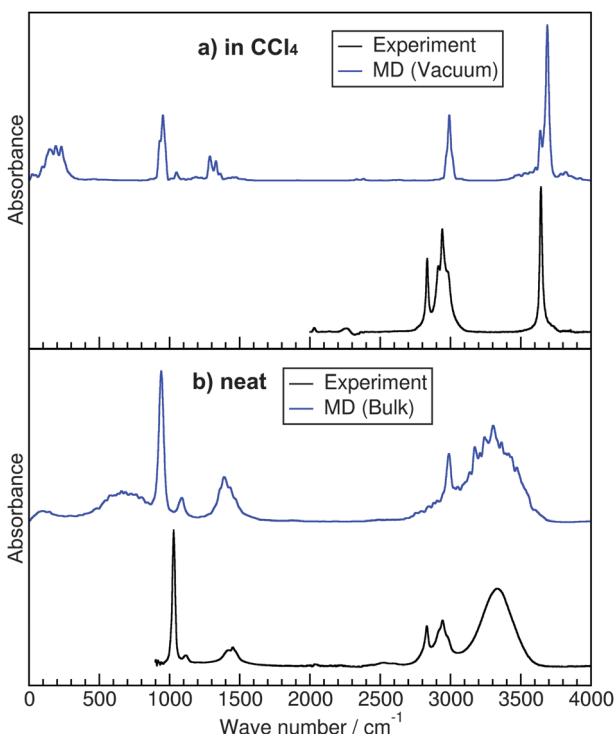


Fig. 2 Experimental IR spectra of methanol: (a) methanol in carbon tetrachloride ($c = 0.005\text{ mol L}^{-1}$, $d = 2\text{ mm}$) compared to AIMD simulation of a single methanol molecule; (b) pure liquid methanol compared to AIMD simulation of the methanol bulk phase.

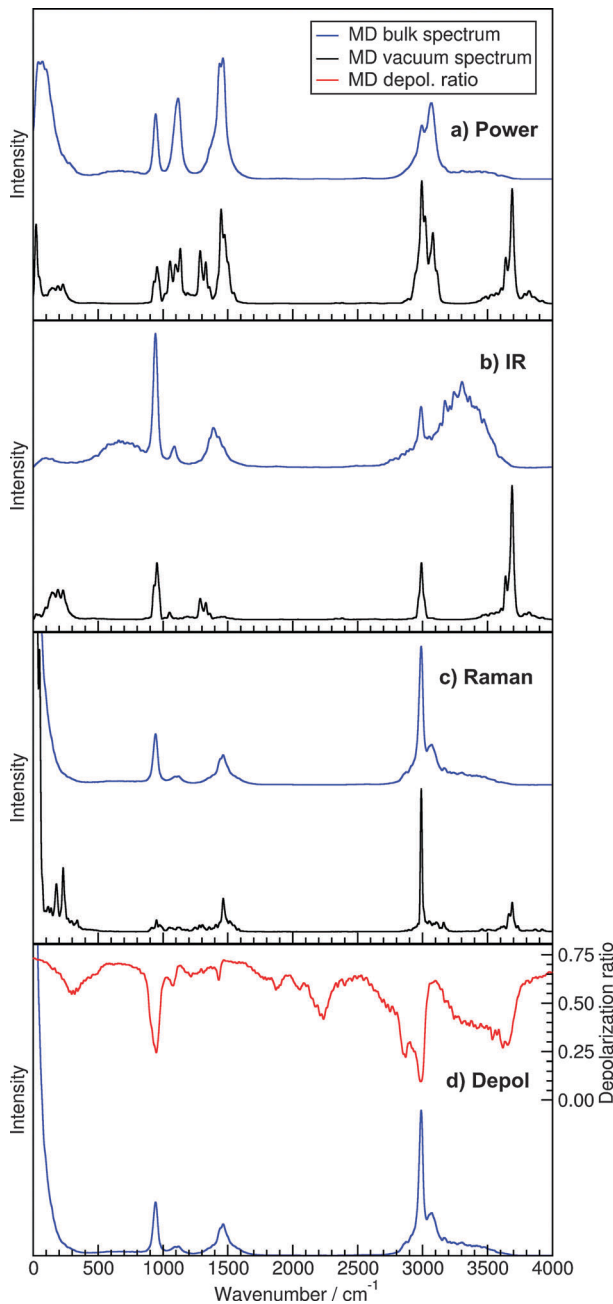


Fig. 3 Spectra for the methanol bulk phase in comparison to a single methanol molecule: (a) power spectra from AIMD simulation; (b) IR spectra from AIMD simulation; (c) Raman spectra from AIMD simulation; (d) Raman depolarization ratio from AIMD simulation of bulk phase with Raman spectrum from AIMD simulation of the bulk phase.

good estimation of the intensities as well as the peak shapes in the experimental Raman spectrum of liquid methanol (see ref. 120 and 122).

4.2 Acetone

In Fig. 4, the spectra for a single acetone molecule are given. Again it is nicely fulfilled that there is a peak in the power spectrum for each normal mode of the static calculation. Similar to methanol, there is a slight shift to higher frequencies

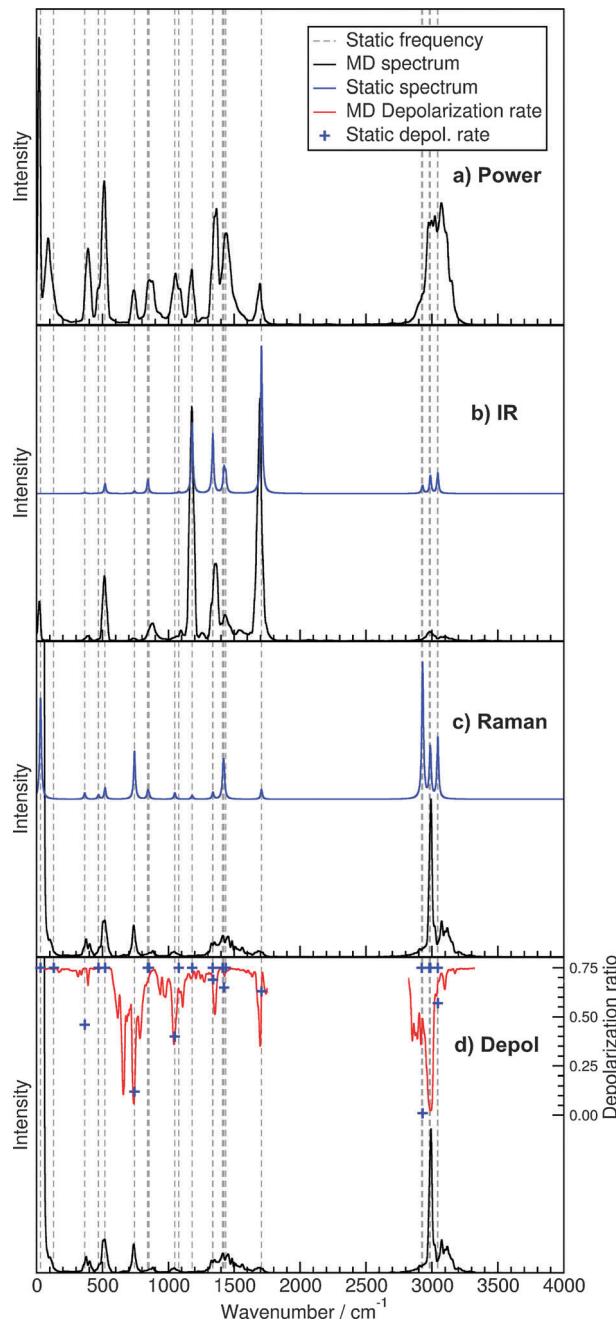


Fig. 4 Spectra of acetone (normal modes from static calculation indicated by dashed vertical lines, static spectra broadened by Lorentzian functions with FWHM of 15 cm^{-1}): (a) power spectrum from AIMD simulation; (b) IR spectra from AIMD simulation and static calculation; (c) Raman spectra from AIMD simulation and static calculation; (d) Raman depolarization ratios from AIMD simulation and static calculation (indicated by crosses) with Raman spectrum from AIMD simulation.

for the band corresponding to the C-H stretching vibrations around 3000 cm^{-1} , but the frequencies of all the other normal modes are reproduced very well by the power spectrum.

The overall shapes of the IR spectra from AIMD and the static calculation coincide very well. Each peak of the static spectrum is reproduced in the AIMD except for the three C-H stretching bands around 3000 cm^{-1} . The situation is however

the same as with methanol since also for acetone, the power spectrum already shows that the C-H stretching vibrations are difficult to separate in the AIMD. The IR spectrum from AIMD features an additional peak at approximately 30 cm^{-1} , which seems to correspond to the normal mode at this frequency. However, this is just an accidental coincidence. As long as the investigated molecule possesses a permanent dipole moment, the AIMD simulation often produces a peak in this frequency region due to the rotation, which also changes the dipole moment with respect to the laboratory coordinate system. Since methanol has a smaller dipole moment than acetone, this effect was not observed in the methanol spectrum. Concerning the IR intensities, both methods are in good agreement, in particular for the C-O stretching vibration at 1700 cm^{-1} , which is characteristic of carbonyl compounds. A notable difference occurs only for the bands at 520 cm^{-1} and 1180 cm^{-1} . The normal mode vectors from the static calculation show that these belong to the two vibrations where the C-C-O angle significantly oscillates. Since the band shape does not necessarily indicate pronounced anharmonicity effects, the deviation probably arises from the basis set difference between the AIMD and the static calculation. In any case, experimental data available in the literature are reproduced reasonably well.^{121,123,124}

The Raman spectra from AIMD and the static calculation are also in good agreement. Each Raman active normal mode of the static calculation is reproduced in the AIMD spectrum. Interestingly, the C-H stretching vibrations are better separated here, but this is due to the high intensity. Considering the strong broadening of the C-H bending vibrations at 1420 cm^{-1} , the Raman intensities predicted by the two methods match very well except for the C-C-O bending mode at 520 cm^{-1} , which is the same problematic one as in the IR spectrum. The normal mode at 30 cm^{-1} cannot be checked since it is covered by the rotation band. The depolarization ratios predicted by the two methods are also in good agreement for most of the bands. Considering again the frequency shift of the C-H stretching vibrations, these are reproduced very well. Important deviations occur however for the C-O stretching vibration at 1700 cm^{-1} , the CH₃ umbrella vibrations at 1340 cm^{-1} and the C-C-C bending mode at 370 cm^{-1} . Since these normal modes show relatively low Raman intensities with broad peaks, the problem potentially is simply a numerical one.

4.3 Nitromethane

The spectra calculated for a single nitromethane molecule are shown in Fig. 5. As for the previous molecules, the peak positions in the power spectrum nicely agree with the frequencies of the normal mode analysis. However, the slight shift of the C-H stretching vibrations to higher frequencies is found again. A remarkable feature of the power spectrum is furthermore the large peak at 860 cm^{-1} , which corresponds to the NO₂ bending vibration. Its large intensity might indicate that the total energy is not fully equipartitioned in the trajectory so that the NO₂ bending mode probably collected excess energy.

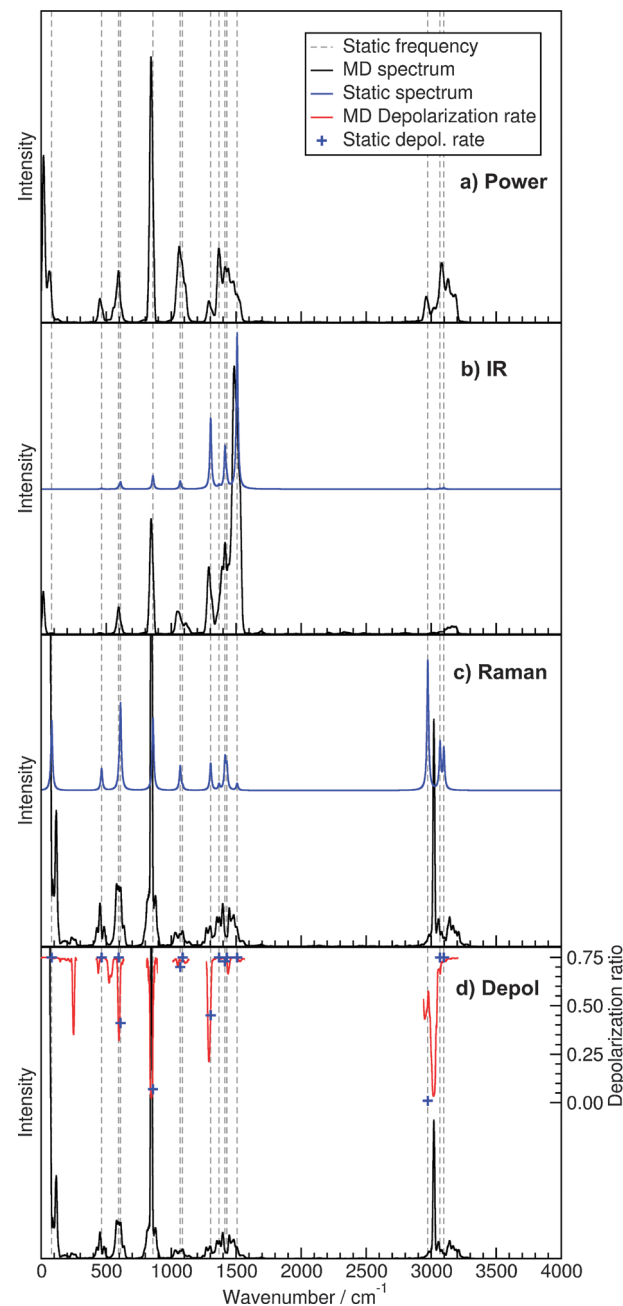


Fig. 5 Spectra of nitromethane (normal modes from static calculation indicated by dashed vertical lines, static spectra broadened by Lorentzian functions with FWHM of 15 cm^{-1}): (a) power spectrum from AIMD simulation; (b) IR spectra from AIMD simulation and static calculation; (c) Raman spectra from AIMD simulation and static calculation; (d) Raman depolarization ratios from AIMD simulation and static calculation (indicated by crosses) with Raman spectrum from AIMD simulation.

The static IR spectrum and the one from AIMD agree again very well. All IR active normal modes from the static calculation are also found in the AIMD spectrum, in particular the anti-symmetric N-O stretching vibration at 1500 cm^{-1} , which is characteristic of the nitro group. The intensity of the C-H bending vibration at 1420 cm^{-1} seems to be too high in the AIMD spectrum, but this is only a consequence of the broader

N–O stretching band so that these two peaks are partially fused there. An important deviation is however the intensity of the NO_2 bending vibration at 860 cm^{-1} , which is significantly higher in the AIMD spectrum. As already indicated by the power spectrum, this normal mode is probably excited too much in the simulation. In this case, the amplitude of the oscillation is too large so that finally the dipole moment derivative is overestimated and the intensity becomes too high. Nevertheless, the calculations are in good agreement with experimental data.¹²⁵

Also the Raman spectra predicted by the two methods coincide nicely. All Raman active normal modes of the static calculation are recovered very well, although it is difficult to individually assign the peaks between 1200 cm^{-1} and 1600 cm^{-1} due to the broadening in the AIMD spectrum. Also the intensities are in very good agreement except for the NO_2 bending vibration at 860 cm^{-1} . As already stated, this normal mode is potentially excited too much so that the intensity is overestimated in the same way as in the IR spectrum. Nevertheless, experimental results are recovered reasonably well.^{125,126} The depolarization ratios for the most intensive Raman bands, the NO_2 bending vibration at 860 cm^{-1} and the C–H stretching vibration at 3000 cm^{-1} , agree very well. Some deviations occur however for the less intensive modes, in particular the C–N stretching vibrations at 610 cm^{-1} and 1300 cm^{-1} . As previously discussed, this is probably a numerical issue.

4.4 Pinacol

For a single pinacol molecule (antiperiplanar conformation), the simulated spectra are shown in Fig. 6. The spectra are more complex because pinacol has more normal modes than the other molecules. This makes the assignment of the peaks in the power spectrum to individual vibrations more difficult. However, it is still possible to draw some general conclusions. As already seen for the other molecules, the C–H stretching vibrations around 3000 cm^{-1} are shifted to higher frequencies in the AIMD simulation. This time, also the O–H stretching vibrations at 3700 cm^{-1} are affected in this way. Nevertheless, the general positions of all other normal modes are reproduced very well. In particular, the frequencies of the relatively isolated normal modes at 650 cm^{-1} , corresponding to the stretching of the central C–C bond, and 80 cm^{-1} , corresponding to the torsion of the central C–C bond, are in very good agreement. Furthermore, it has to be kept in mind that the static calculation relies on a fixed conformation of the molecule whereas several different conformations are sampled in AIMD. This concerns particularly the hydroxyl groups, which more or less rotate freely in our trajectory at a temperature of 400 K. The small intensity of the O–H stretching vibrations in the power spectrum potentially indicates however that these normal modes are excited far too less in the AIMD simulation.

In the IR spectra, the general shape is again in good agreement and each peak of the static calculation is recovered in the AIMD spectrum. Some pronounced differences occur however for the intensities. The most intensive peak in the

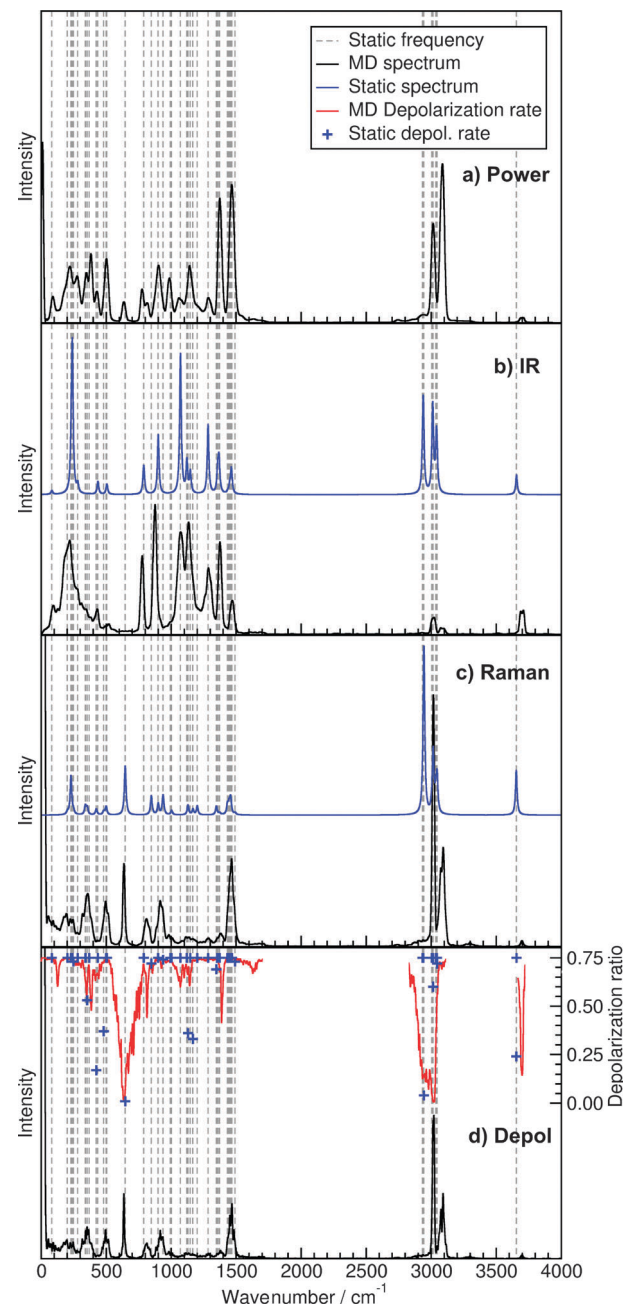


Fig. 6 Spectra of pinacol (normal modes from static calculation indicated by dashed vertical lines, static spectra broadened by Lorentzian functions with FWHM of 15 cm^{-1}): (a) power spectrum from AIMD simulation; (b) IR spectra from AIMD simulation and static calculation; (c) Raman spectra from AIMD simulation and static calculation; (d) Raman depolarization ratios from AIMD simulation and static calculation (indicated by crosses) with Raman spectrum from AIMD simulation.

static spectrum belongs to the torsion of the C–O bonds at 240 cm^{-1} . Considering the significant broadening of this band in the AIMD spectrum, which was also observed for the hydroxyl group in methanol, this vibration is reproduced in the right way. A similar argument holds also for the C–O–H bending vibrations at 1070 cm^{-1} and 1280 cm^{-1} , although the broadening is less pronounced there. However, the reason for the differences

in the C-H stretching vibrations remains unclear. The power spectrum indicates that anharmonicity plays a significant role, but potentially the deviations could be caused by the basis set difference.

The Raman spectra obtained from the two methods are in good agreement as well. As before, each peak of the static calculation can be found in the AIMD spectrum. Except for the O-H stretching vibration, also the intensities are recovered in the right way. In particular for the C-H stretching vibrations, this is in contrast to the IR spectrum. There are some minor differences in the C-H deformation at 1450 cm^{-1} and the torsion of the C-O bonds at 230 cm^{-1} . However, these are caused by the anharmonicity, which is indicated by the shoulder in the power spectrum above 1500 cm^{-1} for the former, and which has been discussed in connection with the IR spectra for the latter. As mentioned before, the O-H stretching mode is very likely too weakly excited, which could explain the difference in the corresponding Raman intensity. Although the IR spectra agree for this band, it is possibly misleading as it has been discussed for the methanol molecule, where the O-H stretching vibration in the AIMD spectrum is much more intensive than in the static calculation due to the anharmonicity. The depolarization ratios predicted by the two methods are in good agreement at least for the most intensive normal modes, namely the C-H stretching vibrations around 3000 cm^{-1} , the C-H deformation modes at 1450 cm^{-1} , and the stretching of the central C-C bond at 650 cm^{-1} . Significant differences occur for the C-H deformation vibrations around 1150 cm^{-1} and the C-C deformation vibrations around 450 cm^{-1} . As discussed for the previous molecules, this is probably a numerical effect due to the low intensities.

An experimental IR spectrum of pinacol in carbon tetrachloride is given in Fig. 7. Although only certain frequency ranges are available due to the solvent absorption, all important bands above 1000 cm^{-1} can be compared. The AIMD spectrum agrees very well with the experiment for the two peaks around 1100 cm^{-1} as well as the three peaks between 1300 cm^{-1} and 1500 cm^{-1} . Just the frequencies of the former group and the first peak of the latter group are estimated to be

too low, but this is very likely a deficiency of the exchange-correlation functional in the underlying electronic structure method. As already presumed in the comparison to the static calculation, the intensities of the C-H stretching vibrations are strongly underestimated in the AIMD spectrum. Also the frequency values of more than 3000 cm^{-1} are higher than those obtained in the experiment. The O-H stretching modes fit better, but their intensities are also slightly too low and the vibrational frequencies are overestimated. Furthermore, the splitting of the two O-H stretching vibrations by 47 cm^{-1} found in the experiment is underestimated in the AIMD simulation. Particularly in the case of the hydroxyl groups, the reason for the deviations is possibly the missing solvent interaction in the AIMD trajectory.

4.5 Temperature influence

A very important parameter in every AIMD simulation within the NVT ensemble is the temperature. Since it determines the amount of energy per vibrational degree of freedom, the oscillation amplitudes are dependent on the temperature. If the system would only consist of purely harmonic oscillators, this would not change the shapes of the spectra, because each vibration would be affected exactly in the same way. In a real-world system however, the oscillation amplitude influences how far the anharmonic region of the potential energy surface is sampled. It is therefore expected that higher simulation temperatures lead to more pronounced anharmonicity effects in all the spectra. To test this supposition, we repeated the simulations of the single methanol molecule for three other temperatures. The corresponding spectra at 10 K , 100 K , 400 K , and 1000 K are compared in Fig. 8.

In principle, all the power spectra show the same information, as they feature peaks at the frequencies of the normal modes. However, there are pronounced differences in the band shapes. At 10 K , the peaks are very sharp and they allow for a clear separation of all normal modes except for the region around 1450 cm^{-1} . This nicely shows that only the harmonic region of the potential energy surface is sampled in this case. With increasing temperature, the peaks get broader and they are smeared so much at 1000 K that it is hard to identify individual peaks. Furthermore, it should be noted that the intensities deviate in particular for the 10 K simulation. This indicates that it is difficult to reach a well equilibrated state with approximately the same amount of energy in every degree of freedom at this temperature due to the slow dynamics.

Apart from the increasingly broadened bands, the IR intensity ratios are very similar at the three higher temperatures. Some deviations occur however at 10 K . As already indicated by the power spectrum, it is difficult to reach sufficient equilibration at this temperature, and this naturally also affects the IR intensities. Another possibility that has to be considered is the missing anharmonicity, since only a very small region of the potential energy surface is sampled. As discussed earlier for the single methanol molecule, anharmonic effects are likely the reason for the large IR intensity of the O-H stretching mode in the AIMD spectrum so this could also explain the lowered intensity of this vibration at 10 K .

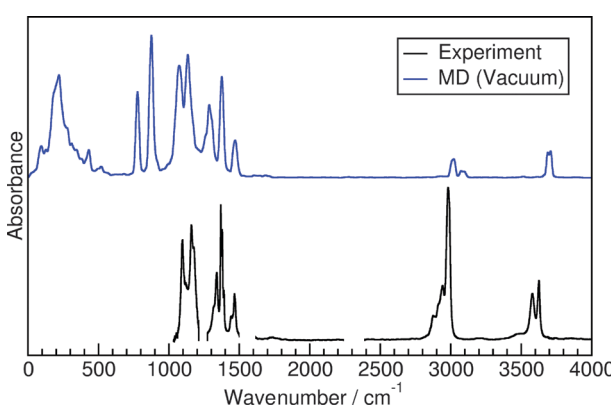


Fig. 7 Experimental IR spectrum of pinacol in carbon tetrachloride ($c = 0.01\text{ mol L}^{-1}$, $d = 2\text{ mm}$) compared to AIMD simulation of a single pinacol molecule.

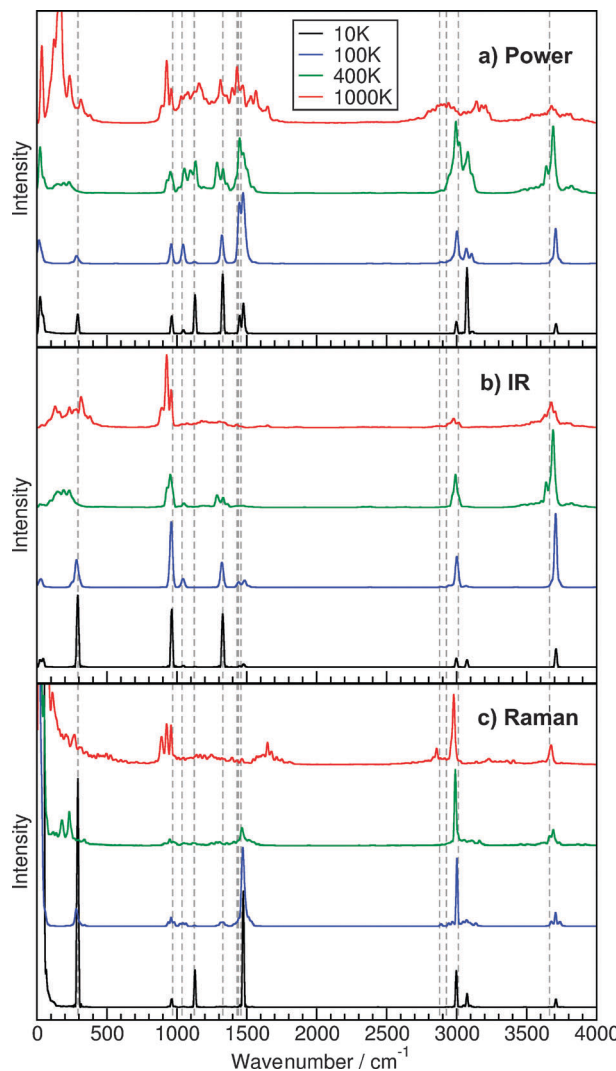


Fig. 8 Spectra of a single methanol molecule at different temperatures: (a) power spectra from AIMD simulation; (b) IR spectra from AIMD simulation; (c) Raman spectra from AIMD simulation.

Similar conclusions can be drawn from the comparison of the Raman spectra, although the differences between the temperatures are more pronounced there. This concerns mainly the C-H deformation modes at 1500 cm^{-1} and the torsion of the C-O bond below 300 cm^{-1} . This is very likely an anharmonicity effect, which has already been discussed in particular for the latter. Furthermore, the Raman spectrum at 1000 K features bands up to 1800 cm^{-1} and at 2850 cm^{-1} , which are not present at lower temperatures. Although there are corresponding peaks in the power spectrum, this is also connected to strong anharmonicity influences and it shows that the simulation at 1000 K is fairly unsuitable to estimate the Raman spectrum of a single methanol molecule.

Summing up, the comparison of the spectra at four different temperatures shows two essential effects. On the one hand, the peaks are very sharp at low temperatures and this allows for a more accurate determination of the peak positions. This provides a particular advantage if the vibrational frequencies are

desired and is therefore of most importance for the power spectrum, where all normal modes appear. On the other hand, higher temperatures are required to sample the anharmonic region of the potential energy surface. As discussed, this is *e.g.* important for the O-H stretching vibration in methanol. Furthermore, it is more difficult to reach sufficient equilibration at lower temperatures and this reduces the reliability of IR and Raman intensities there.

4.6 Simulation time influence

Another important parameter is the total length of the trajectory. Since the computational requirements linearly increase with the trajectory length, an interesting question is the minimal number of steps needed to get reasonable spectra. To investigate this, we cut the trajectory of the single methanol molecule after certain timesteps and re-evaluated the spectra from the remaining shorter trajectories. The corresponding results are compared in Fig. 9.

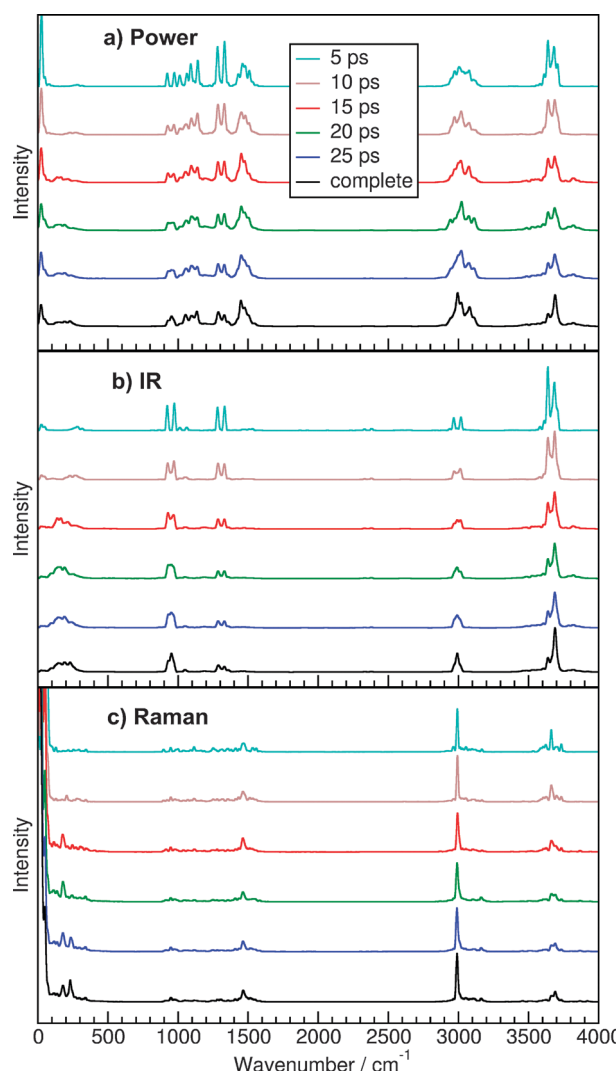


Fig. 9 Spectra of a single methanol molecule at different simulation times: (a) power spectra from AIMD simulation; (b) IR spectra from AIMD simulation; (c) Raman spectra from AIMD simulation.

A common feature of all the spectra is that after 5 ps of simulation time, the general peak positions are reproduced in the right way and the intensity ratios are in qualitative agreement with the converged spectrum. However, many bands are split up due to the poor sampling and they appear as several separate peaks although they correspond only to a single normal mode. This particularly concerns the power spectrum and the IR spectrum between 800 cm^{-1} and 1600 cm^{-1} as well as the C-H stretching band in the IR spectrum around 3000 cm^{-1} . With increasing simulation time, the sampling is improved and the splitting is lifted. Also with longer simulations, the peak shapes converge so that there are only slight changes from 20 ps to 25 ps and nearly no changes from 25 ps to 30 ps in the case of the single methanol molecule. This shows that a simulation time of 20 ps would be sufficient for qualitatively correct results in this example, since reasonable vibrational frequencies and intensity ratios are available after that.

If the same investigation is carried out for the bulk phase trajectory containing 16 methanol molecules, an even faster convergence of the spectra is found. In this case, qualitatively correct results can be obtained after 10 ps and there are nearly no visible changes in the peak shapes after 20 ps. Also the band splitting effect already has vanished at 5 ps. This difference to the single molecule case is simply connected to the fact that not only a longer simulation, but also a larger number of molecules present in the system improves the sampling.

5 Conclusion

In this work, we demonstrated the calculation of vibrational spectra from AIMD simulations *via* time-correlation functions. In particular, we presented mass-weighted power spectra, IR spectra, and Raman spectra with corresponding depolarization ratios for four test systems. Mostly, isolated molecules in gas phase were considered, since this allowed for a comparison of the AIMD results to static calculations with standard quantum chemistry programs, which rely on the harmonic approximation. In doing so, a very good general agreement of these two basically different approaches was found. However, it was observed that AIMD simulations intrinsically account for certain anharmonicity effects and it was shown that this leads to important improvements with respect to the experiment in certain cases, *e.g.* the O-H stretching vibration in methanol.

A major advantage of the AIMD approach is its straightforward applicability to bulk systems so that vibrational spectra of liquid phases become accessible. Although we only studied a pure methanol bulk phase here, we were able to accurately reproduce the experimental data of liquid methanol in terms of peak intensities as well as band shapes. The approach we have chosen for the calculation of dipole moments and polarizabilities is based on maximally localized Wannier functions and this provides the possibility to determine these properties also for the individual molecules in a bulk phase system. This is of particular interest for studies of solute molecules since the pure solute spectrum under the full solvent influence can be investigated in this way.

Furthermore, we studied the influence of the temperature in the AIMD simulation, since this determines how far the anharmonic region of the potential energy surface is sampled. It was shown that low temperatures lead to sharp peaks so that vibrational frequencies can accurately be determined from the peak positions. This is mainly of interest for power spectra, but if many normal modes are close in frequency, IR and Raman spectra can also be useful since the selection rules reduce the number of visible vibrations there. To include anharmonicity effects, it is more convenient to simulate at room temperature or slightly above. This also facilitates to reach sufficient equilibration, which is of particular importance for reliable IR and Raman intensities.

Moreover, we investigated the simulation time needed to obtain reasonable spectra. Although there is no general value since the sampling rate also depends on the number of molecules in the system, we found that a trajectory of 20 ps is sufficient for qualitatively correct results in the case of a single methanol molecule. In bulk phase systems containing several molecules of the same type, the necessary simulation time is even shorter.

Finally, we can state that the prediction of vibrational spectra by AIMD simulations provides a very important method complementary to static approaches. Although it is computationally more demanding than static calculations, it provides superior results when anharmonicity effects play a significant role. The main advantage is however the applicability to bulk systems so that vibrational spectra of liquid phases can be studied.

Acknowledgements

This work was supported by the DFG, in particular by the project KI-768/7-1 and the SFB 813 "Chemistry at spin centers".

References

- 1 A. Barth, *Biochim. Biophys. Acta, Bioenerg.*, 2007, **1767**, 1073–1101.
- 2 T. D. Fridgen, *Mass Spectrom. Rev.*, 2009, **28**, 586–607.
- 3 T. Deckert-Gaudig and V. Deckert, *Curr. Opin. Chem. Biol.*, 2011, **15**, 719–724.
- 4 R. Bhargava, *Appl. Spectrosc.*, 2012, **66**, 1091–1120.
- 5 A. B. S. Elliott, R. Horvath and K. C. Gordon, *Chem. Soc. Rev.*, 2012, **41**, 1929–1946.
- 6 D. Cialla, A. März, R. Böhme, F. Theil, K. Weber, M. Schmitt and J. Popp, *Anal. Bioanal. Chem.*, 2012, **403**, 27–54.
- 7 S. Pahlow, A. März, B. Seise, K. Hartmann, I. Freitag, E. Kämmer, R. Böhme, V. Deckert, K. Weber, D. Cialla and J. Popp, *Eng. Life Sci.*, 2012, **12**, 131–143.
- 8 J. Lindner and P. Vöhringer, *Femtosecond Vibrational Spectroscopies and Applications to Hydrogen-Bond Dynamics in Condensed Phases*, Wiley-VCH Verlag GmbH & Co. KGaA, 2012, pp. 643–686.
- 9 T. Weymuth, M. P. Haag, K. Kiewisch, S. Luber, S. Schenk, C. R. Jacob, C. Herrmann, J. Neugebauer and M. Reiher, *J. Comput. Chem.*, 2012, **33**, 2186–2198.

- 10 N. S. Bieler, M. P. Haag, C. R. Jacob and M. Reiher, *J. Chem. Theory Comput.*, 2011, **7**, 1867–1881.
- 11 F. Pfeiffer and G. Rauhut, *J. Phys. Chem. A*, 2011, **115**, 11050–11056.
- 12 V.-M. Rodriguez-Betancourt, V.-M. Quezada-Navarro, M. Neff and G. Rauhut, *Chem. Phys.*, 2011, **387**, 1–4.
- 13 S. Heislbetz and G. Rauhut, *J. Chem. Phys.*, 2010, **132**, 124102.
- 14 F. Neese, *Coord. Chem. Rev.*, 2009, **253**, 526–563.
- 15 S. Luber and M. Reiher, *ChemPhysChem*, 2009, **10**, 2049–2057.
- 16 S. Luber, J. Neugebauer and M. Reiher, *J. Chem. Phys.*, 2009, **130**, 064105.
- 17 C. R. Jacob and M. Reiher, *J. Chem. Phys.*, 2009, **130**, 084106.
- 18 J. J. Lee, S. Höfener, W. Klopper, T. N. Wassermann and M. A. Suhm, *J. Phys. Chem. C*, 2009, **113**, 10929–10938.
- 19 G. Rauhut, G. Knizia and H.-J. Werner, *J. Chem. Phys.*, 2009, **130**, 054105.
- 20 R. I. Ovsyannikov, W. Thiel, S. N. Yurchenko, M. Carvajal and P. Jensen, *J. Mol. Spectrosc.*, 2008, **252**, 121–128.
- 21 M. Kumarasiri, C. Swalina and S. Hammes-Schiffer, *J. Phys. Chem. B*, 2007, **111**, 4653–4658.
- 22 T. Hrenar, H.-J. Werner and G. Rauhut, *J. Chem. Phys.*, 2007, **126**, 134108.
- 23 T. Petrenko and F. Neese, *J. Chem. Phys.*, 2007, **127**, 164319.
- 24 M. A. Mroginski, F. Mark, W. Thiel and P. Hildebrandt, *Biophys. J.*, 2007, **93**, 1885–1894.
- 25 M. Dierksen and S. Grimme, *J. Phys. Chem. A*, 2004, **108**, 10225–10237.
- 26 M. Dierksen and S. Grimme, *J. Chem. Phys.*, 2004, **120**, 3544–3554.
- 27 J. Neugebauer and M. Reiher, *J. Phys. Chem. A*, 2004, **108**, 2053–2061.
- 28 J. Neugebauer and B. A. Hess, *J. Chem. Phys.*, 2003, **118**, 7215–7225.
- 29 F. Pawłowski, A. Halkier, P. Jorgensen, K. L. Bak, T. Helgaker and W. Klopper, *J. Chem. Phys.*, 2003, **118**, 2539–2549.
- 30 J. Neugebauer, M. Reiher, C. Kind and B. A. Hess, *J. Comput. Chem.*, 2002, **23**, 895–910.
- 31 P. Borowski, *J. Phys. Chem. A*, 2012, **116**, 3866–3880.
- 32 J. P. Merrick, D. Moran and L. Radom, *J. Phys. Chem. A*, 2007, **111**, 11683–11700.
- 33 Y. Tantirungrotechai, K. Phanasant, S. Roddecha, P. Surawatanawong, V. Sutthikhum and J. Limtrakul, *THEOCHEM*, 2006, **760**, 189–192.
- 34 P. Deglmann, F. Furche and R. Ahlrichs, *Chem. Phys. Lett.*, 2002, **362**, 511–518.
- 35 D. Rappoport and F. Furche, *J. Chem. Phys.*, 2007, **126**, 201104.
- 36 J.-h. Shi and C.-h. Fan, *Spectrochim. Acta, Part A*, 2012, **95**, 230–234.
- 37 A. Kobayashi, K. Osawa, M. Terazima and Y. Kimura, *Phys. Chem. Chem. Phys.*, 2012, **14**, 13676–13683.
- 38 X. Ji, Y. Li, J. Zheng and Q. Liu, *Mater. Chem. Phys.*, 2011, **130**, 1151–1155.
- 39 R. Vianello and J. Mavri, *New J. Chem.*, 2012, **36**, 954–962.
- 40 A. D. Kulkarni, D. Rai, L. J. Bartolotti and R. K. Pathak, *J. Chem. Phys.*, 2009, **131**, 054310.
- 41 R. Car and M. Parrinello, *Phys. Rev. Lett.*, 1985, **55**, 2471–2474.
- 42 B. Kirchner, P. Dio and J. Hutter, *Multiscale Molecular Methods in Applied Chemistry*, Springer, Berlin, Heidelberg, 2012, vol. 307, pp. 109–153.
- 43 J. Thar, W. Reckien and B. Kirchner, *Atomistic Approaches in Modern Biology*, Springer, Berlin, Heidelberg, 2007, vol. 268, pp. 133–171.
- 44 J. Thar, M. Brehm, A. P. Seitsonen and B. Kirchner, *J. Phys. Chem. B*, 2009, **113**, 15129–15132.
- 45 M. Brehm, H. Weber, A. S. Pensado, A. Stark and B. Kirchner, *Phys. Chem. Chem. Phys.*, 2012, **14**, 5030–5044.
- 46 M. Brüssel, M. Brehm, A. S. Pensado, F. Malberg, M. Ramzan, A. Stark and B. Kirchner, *Phys. Chem. Chem. Phys.*, 2012, **14**, 13204–13215.
- 47 A. S. Pensado, M. Brehm, J. Thar, A. P. Seitsonen and B. Kirchner, *ChemPhysChem*, 2012, **13**, 1845–1853.
- 48 F. Malberg, A. S. Pensado and B. Kirchner, *Phys. Chem. Chem. Phys.*, 2012, **14**, 12079–12082.
- 49 D. Marx, *ChemPhysChem*, 2006, **7**, 1848–1870.
- 50 J. Schmidt, J. VandeVondele, I.-F. W. Kuo, D. Sebastiani, J. I. Siepmann, J. Hutter and C. J. Mundy, *J. Phys. Chem. B*, 2009, **113**, 11959–11964.
- 51 R. Futrelle and D. McGinty, *Chem. Phys. Lett.*, 1971, **12**, 285–287.
- 52 M.-P. Gaigeot, M. Martinez and R. Vuilleumier, *Mol. Phys.*, 2007, **105**, 2857–2878.
- 53 G. Mathias and M. D. Baer, *J. Chem. Theory Comput.*, 2011, **7**, 2028–2039.
- 54 J. Horníček, P. Kaprálová and P. Bouř, *J. Chem. Phys.*, 2007, **127**, 084502.
- 55 J. Hudecová, K. H. Hopmann and P. Bouř, *J. Phys. Chem. B*, 2012, **116**, 336–342.
- 56 P. L. Silvestrelli, M. Bernasconi and M. Parrinello, *Chem. Phys. Lett.*, 1997, **277**, 478–482.
- 57 M. Bernasconi, P. L. Silvestrelli and M. Parrinello, *Phys. Rev. Lett.*, 1998, **81**, 1235–1238.
- 58 R. Iftimie and M. E. Tuckerman, *J. Chem. Phys.*, 2005, **122**, 214508.
- 59 V. Buch, F. Mohamed, M. Parrinello and J. P. Devlin, *J. Chem. Phys.*, 2007, **126**, 074503.
- 60 V. Buch, F. Mohamed, M. Parrinello and J. P. Devlin, *J. Chem. Phys.*, 2007, **126**, 021102.
- 61 J. Devlin, V. Buch, F. Mohamed and M. Parrinello, *Chem. Phys. Lett.*, 2006, **432**, 462–467.
- 62 M.-P. Gaigeot and M. Sprik, *J. Phys. Chem. B*, 2003, **107**, 10344–10358.
- 63 J.-W. Handgraaf, E. J. Meijer and M.-P. Gaigeot, *J. Chem. Phys.*, 2004, **121**, 10111–10119.
- 64 M.-P. Gaigeot, R. Vuilleumier, M. Sprik and D. Borgis, *J. Chem. Theory Comput.*, 2005, **1**, 772–789.
- 65 M.-P. Gaigeot, *J. Phys. Chem. A*, 2008, **112**, 13507–13517.
- 66 A. Cimas, P. Maitre, G. Ohanessian and M.-P. Gaigeot, *J. Chem. Theory Comput.*, 2009, **5**, 2388–2400.

- 67 M.-P. Gaigeot, N. A. Besley and J. D. Hirst, *J. Phys. Chem. B*, 2011, **115**, 5526–5535.
- 68 R. D. King-Smith and D. Vanderbilt, *Phys. Rev. B: Condens. Matter Mater. Phys.*, 1993, **47**, 1651–1654.
- 69 R. Resta, *Rev. Mod. Phys.*, 1994, **66**, 899–915.
- 70 N. Marzari and D. Vanderbilt, *Phys. Rev. B: Condens. Matter Mater. Phys.*, 1997, **56**, 12847–12865.
- 71 P. L. Silvestrelli and M. Parrinello, *Phys. Rev. Lett.*, 1999, **82**, 3308–3311.
- 72 P. L. Silvestrelli and M. Parrinello, *J. Chem. Phys.*, 1999, **111**, 3572–3580.
- 73 B. Kirchner and J. Hutter, *J. Chem. Phys.*, 2004, **121**, 5133–5142.
- 74 J.-H. Choi, J.-S. Kim and M. Cho, *J. Chem. Phys.*, 2005, **122**, 174903.
- 75 K. Kwac, K.-K. Lee, J. B. Han, K.-I. Oh and M. Cho, *J. Chem. Phys.*, 2008, **128**, 105106.
- 76 M. Aida and M. Dupuis, *THEOCHEM*, 2003, **633**, 247–255.
- 77 A. Miani, S. Raugei, P. Carloni and M. S. Helfand, *J. Phys. Chem. B*, 2007, **111**, 2621–2630.
- 78 A. Miani, M. S. Helfand and S. Raugei, *J. Chem. Theory Comput.*, 2009, **5**, 2158–2172.
- 79 K. Hermansson, S. Knuts and J. Lindgren, *J. Chem. Phys.*, 1991, **95**, 7486–7496.
- 80 R. Eggenberger, S. Gerber, H. Huber, D. Searles and M. Welker, *J. Chem. Phys.*, 1992, **97**, 5898–5904.
- 81 A. Putrino, D. Sebastiani and M. Parrinello, *J. Chem. Phys.*, 2000, **113**, 7102–7109.
- 82 A. Putrino and M. Parrinello, *Phys. Rev. Lett.*, 2002, **88**, 176401.
- 83 M. Pagliai, C. Cavazzoni, G. Cardini, G. Erbacci, M. Parrinello and V. Schettino, *J. Chem. Phys.*, 2008, **128**, 224514.
- 84 R. Mazzarello, S. Caravati, S. Angioletti-Uberti, M. Bernasconi and M. Parrinello, *Phys. Rev. Lett.*, 2010, **104**, 085503.
- 85 M. Brehm and B. Kirchner, *J. Chem. Inf. Model.*, 2011, **51**, 2007–2023.
- 86 N. Wiener, *Acta Math.*, 1930, **55**, 117–258.
- 87 A. Khintchine, *Math. Ann.*, 1934, **109**, 604–615.
- 88 K. Wendler, M. Brehm, F. Malberg, B. Kirchner and L. Delle Site, *J. Chem. Theory Comput.*, 2012, **8**, 1570–1579.
- 89 D. A. A. McQuarrie, *Statistical Mechanics*, Univ. Science Books, 2000.
- 90 J. Borysow, M. Moraldi and L. Frommhold, *Mol. Phys.*, 1985, **56**, 913–922.
- 91 J. S. Bader and B. J. Berne, *J. Chem. Phys.*, 1994, **100**, 8359–8366.
- 92 D. A. Long, *The Raman Effect: A Unified Treatment of the Theory of Raman Scattering by Molecules*, John Wiley & Sons, 2002.
- 93 R. Iftimie and M. E. Tuckerman, *Angew. Chem., Int. Ed.*, 2006, **45**, 1144–1147.
- 94 J. VandeVondele, M. Krack, F. Mohamed, M. Parrinello, T. Chassaing and J. Hutter, *Comput. Phys. Commun.*, 2005, **167**, 103–128.
- 95 CP2K developers group, <http://www.cp2k.org/>.
- 96 J. VandeVondele and J. Hutter, *J. Chem. Phys.*, 2003, **118**, 4365–4369.
- 97 A. D. Becke, *Phys. Rev. A: At., Mol., Opt. Phys.*, 1988, **38**, 3098–3100.
- 98 C. Lee, W. Yang and R. G. Parr, *Phys. Rev. B: Condens. Matter Mater. Phys.*, 1988, **37**, 785–789.
- 99 S. Grimme, J. Antony, S. Ehrlich and H. Krieg, *J. Chem. Phys.*, 2010, **132**, 154104.
- 100 J. VandeVondele and J. Hutter, *J. Chem. Phys.*, 2007, **127**, 114105.
- 101 S. Goedecker, M. Teter and J. Hutter, *Phys. Rev. B: Condens. Matter Mater. Phys.*, 1996, **54**, 1703–1710.
- 102 C. Hartwigsen, S. Goedecker and J. Hutter, *Phys. Rev. B: Condens. Matter Mater. Phys.*, 1998, **58**, 3641–3662.
- 103 M. Krack, *Theor. Chem. Acc.*, 2005, **114**, 145–152.
- 104 S. Nosé, *J. Chem. Phys.*, 1984, **81**, 511–519.
- 105 S. Nosé, *Mol. Phys.*, 1984, **52**, 255–268.
- 106 G. J. Martyna, M. L. Klein and M. Tuckerman, *J. Chem. Phys.*, 1992, **97**, 2635–2643.
- 107 R. Ahlrichs, M. Bär, M. Häser, H. Horn and C. Kölmel, *Chem. Phys. Lett.*, 1989, **162**, 165–169.
- 108 O. Treutler and R. Ahlrichs, *J. Chem. Phys.*, 1995, **102**, 346–354.
- 109 K. Eichkorn, O. Treutler, H. öhm, M. Häser and R. Ahlrichs, *Chem. Phys. Lett.*, 1995, **242**, 652–660.
- 110 K. Eichkorn, F. Weigend, O. Treutler and R. Ahlrichs, *Theor. Chem. Acc.*, 1997, **97**, 119–124.
- 111 F. Weigend, *Phys. Chem. Chem. Phys.*, 2006, **8**, 1057–1065.
- 112 M. Sierka, A. Hogekamp and R. Ahlrichs, *J. Chem. Phys.*, 2003, **118**, 9136–9148.
- 113 F. Furche and R. Ahlrichs, *J. Chem. Phys.*, 2002, **117**, 7433–7447.
- 114 F. Furche and R. Ahlrichs, *J. Chem. Phys.*, 2004, **121**, 12772–12773.
- 115 D. Rappoport and F. Furche, *J. Chem. Phys.*, 2005, **122**, 064105.
- 116 F. Weigend and R. Ahlrichs, *Phys. Chem. Chem. Phys.*, 2005, **7**, 3297–3305.
- 117 Grace, (c) 1996–2008 Grace Development Team, see <http://plasma-gate.weizmann.ac.il/Grace>.
- 118 C. D. Keefe, E. A. L. Gillis and L. MacDonald, *J. Phys. Chem. A*, 2009, **113**, 2544–2550.
- 119 M. Falk and E. Whalley, *J. Chem. Phys.*, 1961, **34**, 1554–1568.
- 120 SDBSWeb: <http://riodb01.ibase.aist.go.jp/sdbs/> (National Institute of Advanced Industrial Science and Technology, accessed November 22, 2012).
- 121 J. E. Bertie and K. H. Michaelian, *J. Chem. Phys.*, 1998, **109**, 6764–6771.
- 122 I. H. Boyaci, H. E. Genis, B. Guven, U. Tamer and N. Alper, *J. Raman Spectrosc.*, 2012, **43**, 1171–1176.
- 123 H. H. Richardson, *J. Phys. Chem.*, 1992, **96**, 5898–5902.
- 124 M. I. Zaki, M. A. Hasan, F. A. Al-Sagheer and L. Pasupulety, *Langmuir*, 2000, **16**, 430–436.
- 125 J. C. Dek, L. K. Iwaki and D. D. Dratt, *J. Phys. Chem. A*, 1999, **103**, 971–979.
- 126 S. Courtecuisse, F. Cansell, D. Fabre and J. P. Petit, *J. Chem. Phys.*, 1998, **108**, 7350–7355.